Lasers in Manufacturing Conference 2023

Laser metal deposition of rene 80 – microstructure and solidification behaviour modelling

Krishnanand Srinivasan[a,*], Andrey Gumenyuk[a], Michael Rethmeier[a,b,c]

[a]*Federal Institute for Materials Research and Testing (BAM), Unter den Eichen 87, 12205 Berlin, Germany*
[b]*Technische Universität Berlin, Institute of Machine Tools and Factory Management, Pascalstraße 8-9, 10587 Berlin, Germany*
[c]*Fraunhofer Institute for Production Systems and Design Technology, Pascalstraße 8-9, 10587 Berlin, Germany*

Abstract

New developments in nickel-based superalloys and production methods, such as the use of additive manufacturing (AM), can result in innovative designs for turbines. It is crucial to understand how the material behaves during the AM process to advance industrial use of these techniques. An analytical model based on reaction-diffusion formalism is developed to better explain the solidification behavior of the material during laser metal deposition (LMD). The well-known Scheil-Gulliver theory has some drawbacks, such as the assumption of equilibrium at the solid-liquid interface, which is addressed by this method. The solidified fractions under the Scheil model and the pure equilibrium model are calculated using CALPHAD simulations. Differential scanning calorimeter is used to measure the heat flow during the solid-liquid phase transformation, the result of which is further converted to solidified fractions. The analytical model is compared with all the other models for validation.

Keywords: laser metal deposition; solidification behaviour; analytical model; nickel-based superalloy; additive manufacturing

1. Introduction

In recent years, Additive Manufacturing (AM) has gained significant recognition in the energy industry due to its capacity to fabricate components, such as combustor gas turbines, that offer enhanced combustion efficiency and reduce the environmental impact of energy production (Sun et al., 2021). Conventionally, the manufacturing of a gas burner, as illustrated in Figure 1, necessitates the assembly of 13 separate pieces and

* Corresponding author. Tel.: +49 3081044813
E-mail address: krishnanand.srinivasan@bam.de

18 weld joints. However, Siemens successfully produced a gas burner in 2017 using Selective Laser Melting (SLM) technology for a gas turbine at a combined cycle gas turbine facility in Germany (Siemens and E.ON Reach Milestone With 3D-printed Burner for SGT-700 Gas Turbine, 19 C.E.)

Fig. 1. 3D printed gas burner for the turbine SGT-700 operating in CCGT plant (Siemens and E.ON Reach Milestone With 3D-printed Burner for SGT-700 Gas Turbine, 19 C.E.)

Nickel-based superalloys like Rene 80 are commonly used in high-temperature applications in the energy and aerospace industries due to their high melting point and oxidation resistance. Rene 80 alloy consists of a solid solution matrix primarily composed of γ phase (Ni) and reinforced with solid solution elements like Co and Cr. The precipitate phase, L_{12} (γ'), possesses a face-centered cubic (FCC) crystal structure, with varying morphologies based on Al and Ti weight percentages. The formation of γ'' precipitates is not expected in Rene 80 due to the absence of Nb (Mignanelli et al., 2017).

The Scheil model, regarded as a non-equilibrium model on a macroscale, assumes local equilibrium at the interface (S-L interface) through stepwise equilibrium computations (Chen et al., 2009). However, this model fails to explain non-equilibrium effects observed during rapid solidification in AM processes, such as solute trapping, where solutes are trapped within the solid phase (Aziz et al., 1982). Hence, we propose an analytical model to describe this non-equilibrium interface kinetics resulting from AM.

2. Analytical model

In this study, we present an analytical model that introduces modifications to the conventional Scheil model by incorporating certain deviations, as illustrated in Figure 2. The fundamental difference lies in the treatment of specific assumptions. In our model, we represent the liquid phase as a cylindrical shape to simplify the analysis. The radius (a) of this cylinder is assumed to be half the distance to the dendritic arm spacing (DAS), providing an estimation of the liquid phase geometry. Surrounding this cylindrical liquid phase is an infinite medium of the solid phase. During the solidification process, as the solid phase grows and the liquid phase recedes, the radius of the cylinder gradually decreases. Ideally, when solidification is complete, the cylinder's radius 'a' would reach zero, indicating a fully solidified system. This assumption allows us to define the model domain with a primary focus on the solid-liquid (S-L) interface. It is important to note that our model is currently designed to describe only the primary phase formation, specifically the γ phase originating from the liquid. We have not considered the formation of any secondary phases, such as MC or γ' phases, in this study.

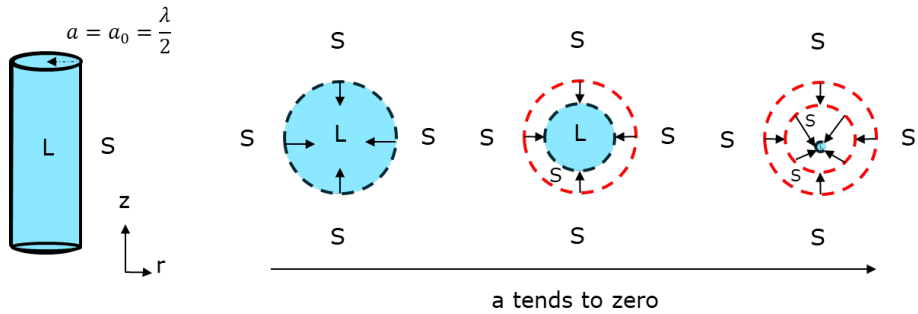

Fig. 2. Model domain assumption

The concentration profile in the liquid is defined using Fick's second law of diffusion using equation 1.

$$\frac{\partial C}{dt} = \frac{1}{r} D \frac{d}{dr}\left(r.\frac{\partial C}{\partial r}\right) \tag{1}$$

The initial solute concentration in the liquid $C = C_0$ determines the initial condition. At the S-L interface, the boundary condition is established by considering the balance between the diffusion process and the reaction kinetics of phase formation and dissolution, as represented by equation 2.

$$-D\frac{\partial C}{dr} = K(T)\,(C_L(T) - C) \tag{2}$$

Where, $C_L(T)$ is the equilibrium liquidus concentration at temperature T and $K(T)$ is the reaction constant. The solution to this boundary value problem (BVP) is a well-known expression derived from the heat exchange between an infinite cylindrical rod surface and the external medium (Carslaw and Jaeger., 1986). The distribution of solute concentration in the liquid phase is given by equation 3.

$$C(r) = C_L(T) + 2(C_0 - C_L(T))\sum_{n=1}^{\infty} \frac{J_1(\gamma_n).e^{\frac{-\gamma_n^2}{a^2}Dt}}{\gamma_n[J_0^2(\gamma_n) + J_1^2(\gamma_n)]}.J_0\left(\gamma_n\frac{r}{a}\right) \tag{3}$$

Where, J_n is the Bessel function and γ_n is the root of Bessel function of the order n. Additionally, the diffusive flow at the interface is also proportional to the changing radius of the liquid domain.

$$\frac{\partial a}{\partial t} = -D\left(\frac{\partial C}{dr}\right) \tag{4}$$

Using the equations (2-4), the time dependent evolution of the radius of liquid phase is formulated.

$$\frac{da}{dt} = 2D[C_L(T) - C_0]\sum_{n=1}^{\infty} \frac{\left(\frac{K(T)}{D}.a\right)^2.e^{\frac{-\gamma_n^2}{a^2}Dt}}{a\left[\gamma_n^2 + \left(\frac{K(T)}{D}.a\right)^2\right]} \tag{5}$$

The model allows for the extraction of the fraction of solid, which can later be compared with other models. Based on the parameter defining the behavior of this analytical solution, it can be limited to two analytical forms, each describing a different scenario.

In the first case, solidification is dominated by the diffusion of the solute element in the liquid. It assumes slow heating and cooling close to equilibrium conditions.

$$\frac{K(T)}{D}.a \gg 1;\ a = a_0 - \gamma_1\sqrt{\frac{\boldsymbol{D} * t}{16}} \tag{6}$$

In the second case, solidification is independent of the diffusion process and is instead dominated by the reaction kinetics at the interface. This condition resembles the rapid cooling involved in AM processes.

$$\frac{K(T)}{D}.a \ll 1;\ a = (2C\boldsymbol{K}^2t^2 + {a_0}^2)^{\frac{1}{2}} - CKT \tag{7}$$

For this work, only the first limiting case (Diffusion dominant) will be considered and further explained.

3. Experimental work

3.1. Material

The material used for the experiments is Nickel superalloy powder, specifically AMDRY Rene 80, with a particle size distribution (d_{50} = 77 µm) suitable for the LMD process. The base plate used is 304 L stainless steel. Table 1 presents the experimental chemical composition of Rene 80 powder as measured by Inductively Coupled Plasma Optical Emission spectroscopy (ICP-OES).

Table 1. Experimental chemical composition of Rene 80 powder

Material	Cr	Co	Ti	W	Mo	Al	Ni
Rene 80 in wt.-%	14.2	9.6	5.1	4.1	4.1	3	bal

3.2. Laser metal deposition

Initially, single line scan LMD experiments were conducted to determine an optimal parameter set. Three parameter sets were selected to produce a thin wall consisting of 20 layers as shown in Table 2. A thin wall is approximately 60 mm long each layer measures about 40-50 µm thick. Bidirectional laser scanning strategy is used.

Table 2. Parameter set used for the LMD experiment

Number	Power P (W)	Scan speed v (mm/min)	Feed rate m (g/min)	Spot diameter s (mm)
RE0601	800	600	15	1.6
RE0602	1000	600	15	1.6
RE0809	800	800	21	2.0

3.3. Differential scanning calorimetry

Thermys One+ was used to perform thermos analytical measurements on the powder Rene 80 sample (Setaram, Caluire, France). The samples were heated in corundum crucibles (100 l) at a slow rate of 0.08 K/sec (to replicate the equilibrium cooling condition) up to a maximum temperature of 1450°C under argon (30 ml/min). The heating and cooling cycle was repeated after cooling to room temperature at a rate of 0.08 K/sec. DSC curves provide information about the typical temperature at which significant phase transformation occurs, such as T_L and T_S.

3.4. Thermodynamic calculations

Calphad calculations were conducted using the TCHEA4 database through ThermoCalc software. Scheil and equilibrium solidifications were calculated for the Rene 80 alloy using the experimentally determined composition. The Scheil-Gulliver equation defines the solute redistribution during solidification of an alloy assuming perfect mixing in the liquid and no diffusion in the solid phase (Pelton et al., 2019).

4. Results and discussions

4.1. Thermo-Calc calculations

The equilibrium phase diagram of the Rene 80 alloy, calculated using Thermo-Calc, is presented in Figure 3a. Under equilibrium conditions, the solidified material is expected to contain γ, γ', and MC-type carbide. The freezing range, which represents the temperature range over which solidification occurs, is approximately 67°C in equilibrium conditions. However, in non-equilibrium conditions, the freezing range increases to around 400°C, which is six times higher than in the equilibrium state. This indicates that solidification takes place over a wider temperature range under non-equilibrium conditions.

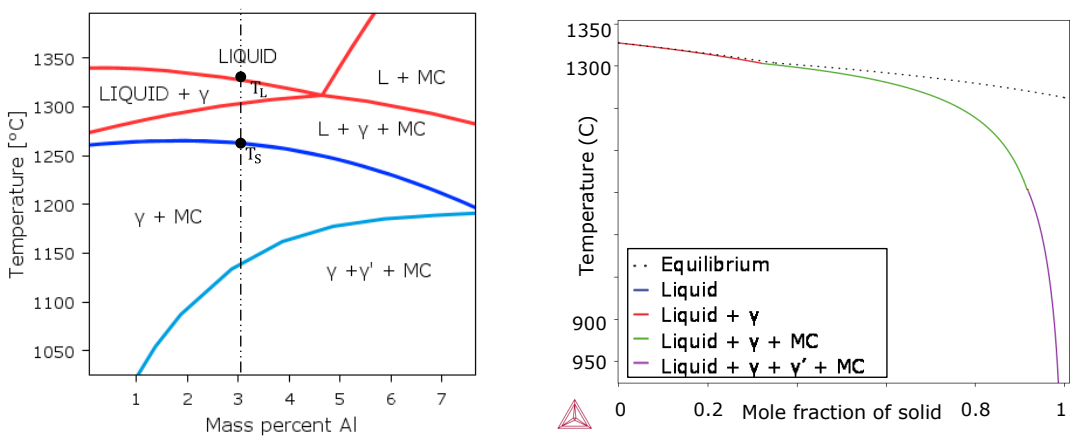

Fig. 3. (a) Equilibrium phase diagram of Rene 80; (b) Scheil calculations of Rene 80

In Figure 3b, the fraction of the dependences of the solid phases on the temperature during solidification is shown for the Rene 80 based on the experimentally measured composition in Table 1. Scheil model is calculated based on the local equilibrium existing between the solid liquid at the interface. No back diffusion of solute is considered. Since the liquid enriched with solute reaches the eutectic composition, the liquid phase can exist at much lower temperature than in the equilibrium condition (represented by dotted lines).

4.2. Differential scanning calorimetry analysis (DSC)

The DSC measurement results are presented in Figure 4, where the condition closely resembles equilibrium. Figure 4a displays the DSC curve, illustrating the exothermic reaction observed during solidification. The baseline is subtracted from the DSC curve and the area of phase transformation is shaded as shown in Figure 4b. The onset of solidification is observed at approximately 1328°C, while completion occurs around 1242°C. The area of total heat flow is quantified, and in Figure 4c, it is converted into the fraction of solidification to facilitate comparison with other models. Notably, the freezing range obtained from the DSC curve is approximately 86°C, slightly higher than what is typically observed in the equilibrium case.

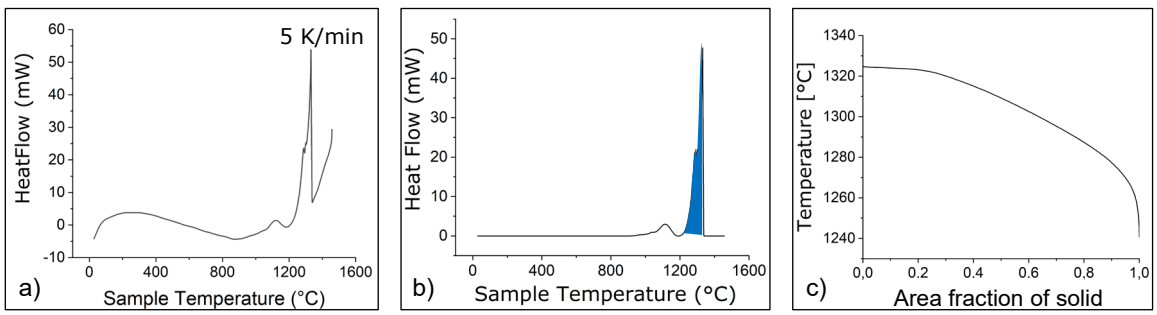

Fig. 4. (a) DSC signal of Rene 80 as a function of temperature; (b) Baseline subtraction (c) The calculated area of solidified fraction

4.3. Microstructure Characterisation

Figure 5 depicts the cross-section of the as-built thin wall, providing insight into its microstructure. The topmost layer exhibits a fine dendritic structure, while the middle layer demonstrates larger grains due to cyclic re-heating and cooling effects. Epitaxial growth results in elongated columnar dendritic grains along the build direction (z) from the substrate. This preferential growth is associated to the opposing heat flux from top to bottom and can be further observed in Figure 6a.

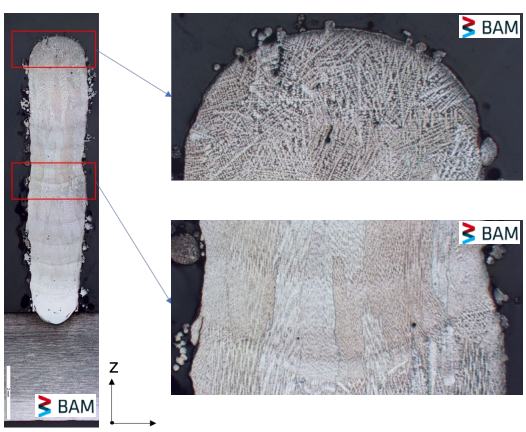

Fig. 5. Cross-sectional microstructure of the as-built thin wall

Figure 6 displays the SEM images of the as-built thin wall. The dendritic arm spacing (DAS) is calculated using image analysis software, where a line is drawn across several dendritic arms and the arm spacing is determined by dividing the number of dendrites by the line length (Figure 6a). The average DAS is estimated to be 6.5 µm ± 0.5 µm, which is used as an input parameter (a_0) in our model. Additionally, Figure 6b and 6c provide evidence of the presence of carbides and γ' precipitates respectively, supporting the Thermo-Calc findings. The size of the γ' precipitates range in between 20 nm and 100nm.

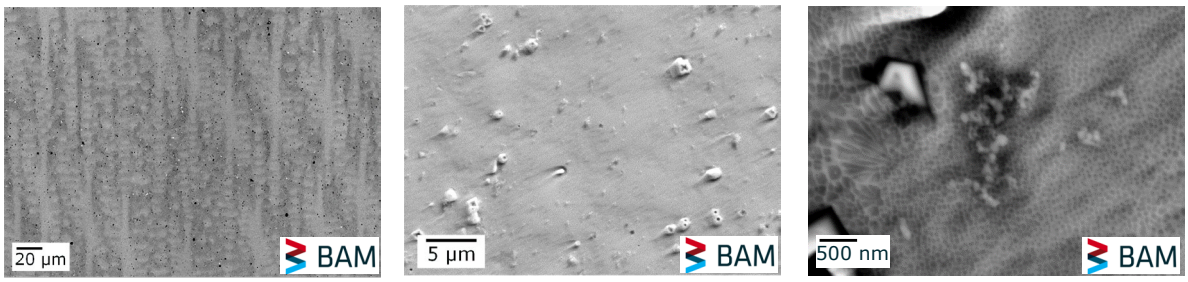

Fig. 6. (a) Columnar dendritic grains; (b) MC carbide precipitates; (c) γ' precipitates

The EDS mapping on a selected area of the Rene 80 samples, shown in Figure 7 reveals the distinct segregation patterns of different elements. Specifically, Al, Co, Cr and Ni are found to segregate predominantly within the columnar dendritic region, while Ti, Mo, W and C tend to segregate in the interdendritic region as shown in Figure 7a and 7b respectively.

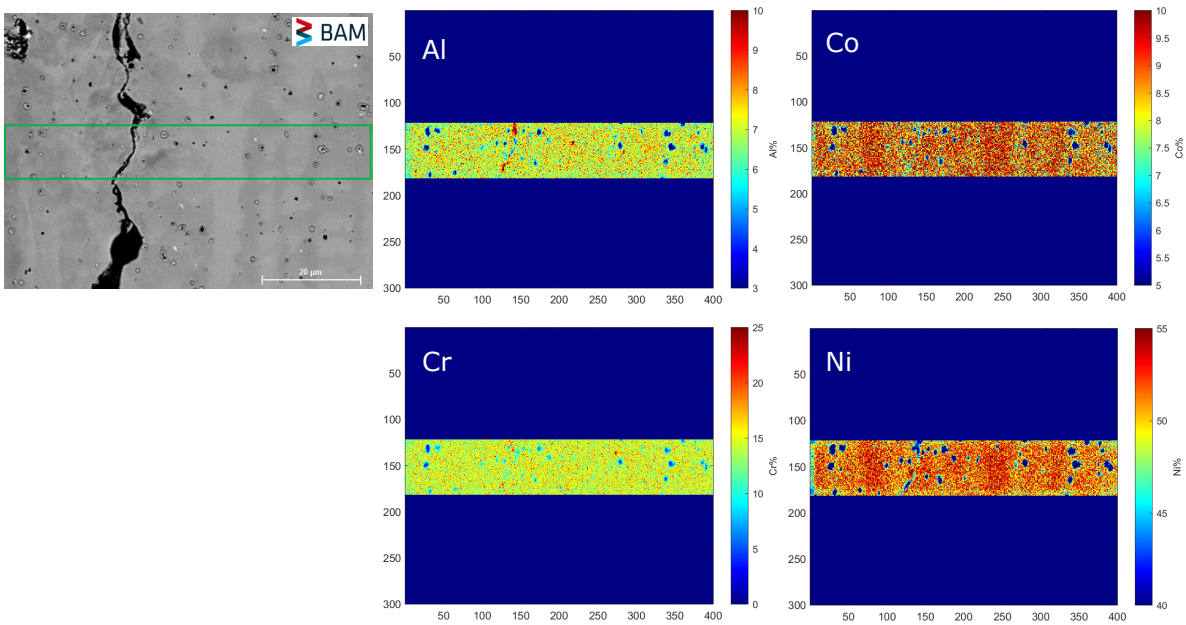

Fig. 7. (a) Elemental segregation of Al, Co, Cr and Ni in columnar dendritic region

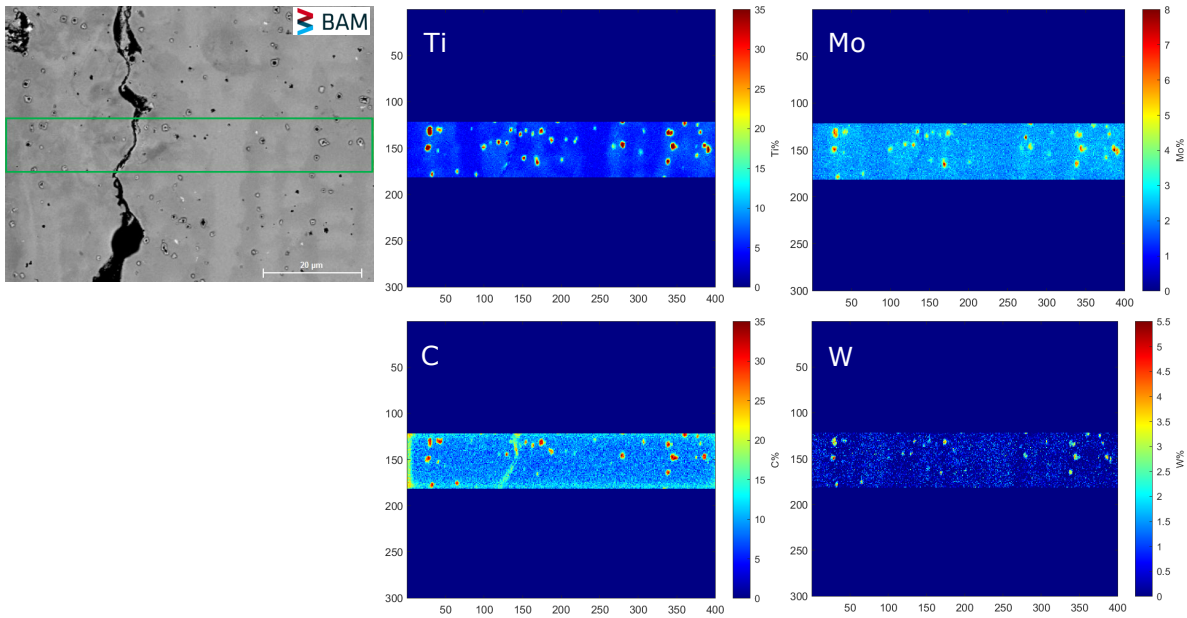

Fig. 7. (b) Elemental segregation of Ti, Mo, W and C in interdendritic region

This elemental segregation behavior can be related to the solidification microstructures forming in the Rene 80 alloy during the additive manufacturing (AM) process. During solidification, the rapid cooling and solidification rates in the columnar dendritic region promote the formation of primary dendrites. The segregation of Al, Co, Cr, and Ni in this region can be attributed to their higher affinity for the dendritic growth and their solubility in the γ phase of the alloy. On the other hand, the interdendritic region experiences slower cooling rates and provides more time for solute diffusion. Consequently, elements such as Ti, Mo, W, and C, which have lower solubility in the γ phase, tend to accumulate in the interdendritic regions due to their limited diffusion within the γ matrix and tends to promote MC carbides in the interdendritic region.

The observed elemental segregation patterns in the columnar dendritic and interdendritic regions are consistent with the known solidification behavior of alloy systems. These findings contribute to our understanding of the microstructural evolution and solidification mechanisms in the Rene 80 alloy during the AM process, providing valuable insights for optimizing the manufacturing parameters and properties of the alloy.

4.4. Validation of the analytical model

The comparison of the analytical model (Diffusion dominant) against other calculated models is presented in Figure 8. The DSC curve obtained at a cooling rate of 0.08 K/s represents the full equilibrium condition characterized by slow cooling. Comparing the diffusion dominant analytical model with the DSC model and the equilibrium model calculated using ThermoCalc, a close agreement is observed between them. However, it is important to note that the Scheil curve, which considers only local interface equilibrium, exhibits the presence of a liquid phase at significantly lower temperatures compared to the other curves.

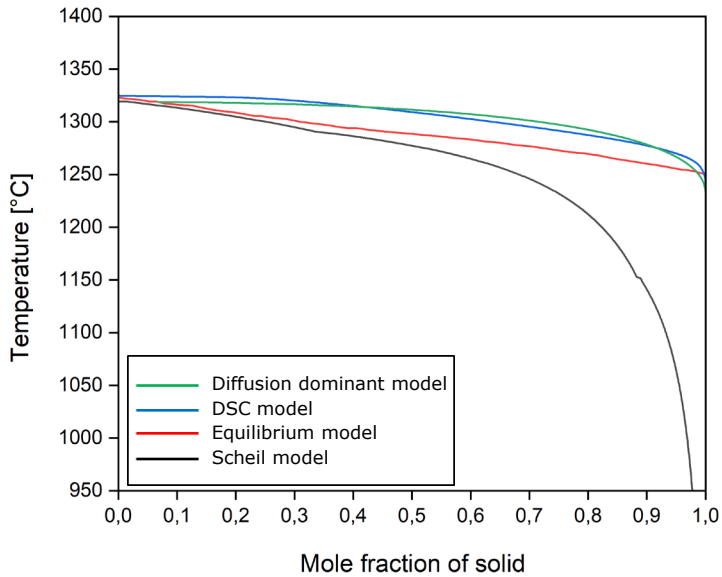

Fig, 8: Validation of the analytical model with other calculated models

While the agreement between the diffusion limiting analytical curve and the equilibrium curve provides confidence in the model's performance under slow cooling conditions, it is essential to address the non-equilibrium solidification associated with rapid cooling during additive manufacturing. By extending the analytical model to consider non-equilibrium solidification (Equation 7), where diffusion is negligible and interface kinetics dominate, the model can capture the complex dynamics of multiple thermal cycles and concurrent phase transformations (Liquid - γ + γ' + MC).

5. Summary and outlook

In this work, an analytical model is proposed to describe the solidification behaviour of Rene 80 alloy in AM process. The proposed model addresses the limitations of existing Scheil model and focuses on the primary phase formation at the solid-liquid interface. To validate our model, we conducted Thermo-Calc calculations, which revealed the presence of γ, γ', and MC phases. Microstructural examination confirmed these findings, highlighting the segregation patterns of elements in both the columnar dendritic and interdendritic regions. These observations provide valuable insights into the microstructural evolution of the Rene 80 alloy during the AM process and shed light on the underlying solidification mechanisms. Model validation was performed by comparing our diffusion-dominant analytical model with the DSC model and equilibrium model. Remarkably, the results demonstrated a good agreement among these models. However, it is important to note that non-equilibrium solidification, which occurs during rapid cooling in the AM process, needs to be further considered. Incorporating non-equilibrium solidification and capturing interface kinetics would significantly enhance the accuracy and applicability of our model in advanced manufacturing processes like AM.

Acknowledgements

We gratefully acknowledge the financial support provided by the Deutsche Forschungsgemeinschaft (DFG) for this project (Project No: 449062083). We would like to express our sincere gratitude to the following individuals from BAM for their valuable contributions: Mr. Hähnel Sören (Department 9.3) for LMD experimental setup; Mr. Romeo Saliwan Neumann (Department 5.1) for SEM-EDS characterization, Dr. Stefan Reinsch (Department 5.6) for DSC measurements, Mr. Mathias Lindemann (Department 7.4) for ICP-OES measurements, and Franziska Lindemann (Department 5.4) for powder characterization.

References

Aziz, M.J., 1982. Model for solute redistribution during rapid solidification. In Journal of Applied Physics (Vol. 53, Issue 2, pp. 1158-1168)

Carslaw, H. S., & Jaeger, J. C., 1986. Conduction of Heat in Solids (p. 202)

Chen, S.-L., Yang, Y., Chen, S.-W., Lu, X.-G., Chang, Y. A., 2009. Solidification Simulation Using Scheil Model in Multicomponent Systems. In Journal of Phase Equilibria and Diffusion (Vol. 30, Issue 5, pp. 429-434)

Mignanelli, M., Jones, G., Pickering, J., Messe, M., Rae, F., Stone, J., 2017. Gamma-gamma prime-gamma double prime dual-superlattice superalloys. In Scripta Materialia (Vol. 136, pp. 136-140)

Pelton, A.D., 2019. Equilibrium and Scheil-Gulliver Solidification. In Phase Diagrams and Thermodynamic Modeling of Solutions (p. 133–148)

Siemens and E.ON reach milestone with 3D-printed burner for SGT-700 gas turbine (By Siemens). (19 C.E., September 18). Retrieved June 24, 2023, from https://press.siemens.com/global/en/pressrelease/siemens-and-eon-reach-milestone-3d-printed-burner-sgt-700-gas-turbine

Sun, C., Wang, Y., Mcmurtrey, M., Jerred, N., Liou, F., Li, J., 2021. Additive Manufacturing for Energy: A review. In Applied Energy (Vol. 282,p. 116041